Nanoscale

Accepted Manuscript

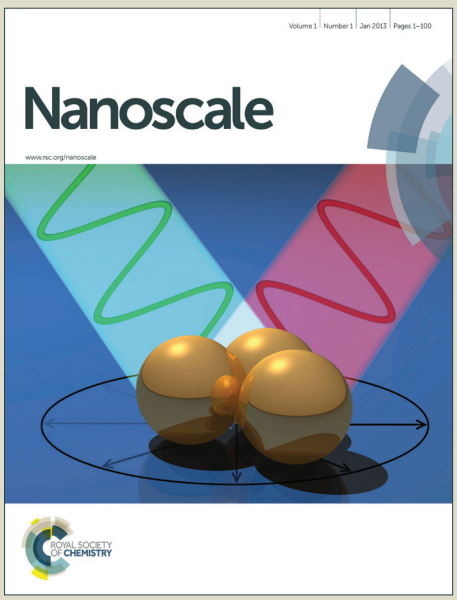

ROYAL SOCIETY OF CHEMISTRY

www.rsc.org/nanoscale

Cite this: DOI: 10.1039/c0xx00000x

www.rsc.org/xxxxxx

ARTICLE TYPE

Graphene nanosheets inserted by silver nanoparticles as zero-dimensinal nanospacers for dye sensitized solar cells

Quanhong Chang [a,b], Zhenping Wang [b], Jinzhong Wang *[a], Yuan Yan [a], Zhoujing Ma [b], Jianxiao Zhu [b], Wangzhou Shi [b], Qi Chen [b], Qingjiang Yu[a], Lei Huang*[b]

Received (in XXX, XXX) Xth XXXXXXXXX 20XX, Accepted Xth XXXXXXXXX 20XX
DOI: 10.1039/b000000x

Three-dimensional Ag nanoparticles/GNs (Ag/GNs) hybrids as highly efficient counter electrode (CE) materials for dye sensitized solar cells (DSSCs) is described, highlighting the Ag nanoparticles as zero-dimensional nanospacers inserting into GNs to lift the interspacing layer between individual GNs. It is demonstrated that, when the hybrids are used as CE materials for DSSCs, compared to their pure GNs, Ag/GNs hybrids without agglomerate have a significant improvement in their electrochemical properties such as high current density, narrow peak-to-peak separation (E_{pp}) and low charge transfer resistance (R_{CT}). The enhancement of electrochemical performance can be attributed to the increased electrode conductivity, an extended interlayer distance and the reduction of the restacking of graphene sheets due to the insertion of metallic Ag nanoparticles into GNs. The DSSC with this hybrid CE exhibited energy conversion efficiency (η) of 7.72% with an open circuit voltage (V_{OC}), short circuit photocurrent density (J_{SC}), and fill factor (FF) of 732 mV, 14.67 mA cm^{-2}, and 71.8%, respectively.

Keywords: graphene nanosheets, silver nanoparticles, zero-dimensional nanospacers, counter electrode, DSSCs

1. Introduction

Dye sensitized solar cells (DSSCs) have considerable potential for next-generation solar cells due to their simple low cost fabrication and high energy conversion efficiency.[1-6] In typical DSSCs, the electrons are injected from photo-oxidized dyes into dye sensitized TiO_2 photoelectrodes, and the resulting oxidized dyes are regenerated by electrolytes. In a typical electrolyte, I^- ions reduce the oxidized dyes, yielding I_3^-, and the resulting I_3^- ions are finally reduced to I^- at a counter electrode (CE).[2-5] Thus, the efficient reduction of I_3^- at CEs is an important requisite to achieve high efficiency DSSCs. For an optimized DSSC, one must choose a CE material with high conductivity, excellent catalytic activity for the reduction of the redox electrolyte, high chemical stability and low cost. Pt-loaded conducting glass has been widely employed as the standard CE for DSSCs due to its high catalytic activity and excellent conductivity.[7-9] However, the poor stability and high cost of Pt means an alternative to it is required for the further development of CEs for DSSCs. Therefore, it is important to explore low cost materials to replace Pt or contain a lower amount of Pt as CEs for DSSCs. For this reason, more attentions have been focused on various materials with low cost as potential alternatives to Pt, including transition metal oxides (NiO) and nitrides (MoN, WN and Fe_2N),[1,3] low-cost quaternary Copper Zinc Tin Sulfide (CZTS) nanocrystals,[4] conducting polyaniline [5]and carbon.[10]

Graphene nanosheets (GNs), as one novel nanostructure of carbon materials, have recently received much interest as CEs for DSSCs because of its two-dimensional structure and unique properties, including high specific surface area, efficient electrocatalytic activity and good electrical conductivity.[10-13] However, the performance of a DSSC with a graphene-based CE is dependent on the structure of graphene. Perfect graphene has an extremely high conductivity, but it may possess a limited number of active sites for I_3^-/I^- electrocatalysis.[13,14] Kavan [11] and Rhee[15]*et al.* demonstrated that the electrocatalytic properties of GNs that take part in a redox reaction are related to the concentration of defects and oxygen-containing groups. Recently, lattice defects such as defective sites at the edge of graphene are considered as electrocatalytic active sites for the reduction of I_3^-.[15] Unfortunately, due to the strong π–π interaction between the large basal planes, GNs tend to easily aggregate, forming multilayered agglomerate.[10,16] This undesirable phenomenon significantly reduces the amount of active defective sites accessibility of I_3^-/I^- insertion into the GNs and further limited the conversion efficiency of DSSCs. To resolve the above problem, one proposed strategy is to place nanospacers between the GNs, exfoliating the graphene agglomerate. Recently, a three-dimensional hybrid carbon framework CE rebuilt by incorporating carbon nanotubes (CNTs) as one-dimensional nanospacers into the layers of GNs was reported by Li-Hsueh Chang *et al.*[17] This hybrid nanoarchitecture prevents the aggregation of the GNs and increases the active sites, thereby obtaining a low charge transfer resistance (R_{CT}) 2.94 Ω cm^2. Jang *et al.* demonstrated a

nanostructure of Pt/graphene composite CE synthesized via the self-assembly of polyelectrolyte, graphene and H_2PtCl_6. The DSSC with this nanostructure CE achieved energy conversion efficiency (η) of 8.91%, comparable to that (8.85%) of the DSSC with the state-of-the-art Pt-based CEs.[18] Importantly, in this hybrid nanostructure composite, Pt nanoparticles can be taken into account as zero-dimensional nanospacers, which efficiently prevent the restacking of graphene layers and increase the defects caused by incorporating Pt into the GNs. Besides, this Pt/graphene CE contained much less Pt than the sputtered-Pt electrode, leading to a dramatic decrease in the DSSC fabrication cost. Additionally, Chien-Te Hsieh *et al*.[19] proposed a novel model that Ag nanorods attached to GNs as anode materials for lithium-ion batteries, in which Ag nanorods as one-dimensional nanospacers induces not only one-dimensional pathway for electronic conductivity but also high accessibility for ionic diffusion. According to these studies in the available literature, hybrid nanoarchitecture CEs with defect-rich GNs to enhance the electrocatalytic activities appear to be a favored alternative to Pt for DSSCs.

To the best of our knowledge, due to the electronic structure of graphene, a higher concentration of defects on the graphene results in a reduced electrical conductivity because of the contribution of decreased range of the delocalized π-electrons in graphene. A point is therefore to strike the appropriate balance between the electrical conductivity and the electrocatalytic properties of the graphene used. Considering the Ag nanoparticles with low cost compared with the Pt, therefore, we selected the use of high conductive Ag nanoparticles as zero-dimensional nanospacers inserting into the layers of GNs, which efficiently prevents the aggregation of GNs in this work. The enhanced electrocatalytic activites for I^-/I_3^- redox couples in DSSCs were demonstrated by cyclic voltammetry (CV) and electrochemical impedance spectroscopy (EIS) analysis. The DSSCs using the optimized Ag nanoparticles/GNs (Ag/GNs) hybrids as CEs exhibited energy conversion efficiency (η) of 7.72% with open circuit voltage (V_{OC}), short circuit current density (J_{SC}), and fill factor (FF) of 730 mV, 14.67 mA cm^{-2}, and 70%, respectively. This expected result is comparable to the performance of DSSCs using state-of-the-art Pt-CEs (η 8.25%).

2. Experiments

2.1 Preparation of GNs and Ag/GNs

Graphite oxide (GO) was obtained by the modified Hummers method as described elsewhere. A homogeneous GO aqueous suspension (0.5 mg/ml) was achieved by dispersing purified GO in DI water with the aid of ultrasonication for 3 h. Then, ammonia was added into the above GO suspension to present in solution at pH 9. Afterward, the GNs solution was fabricated when 40 ml yellow brown GO suspension was loaded into a quartz tube for the pulsed laser reduction, as described in our report.[20] In this work, the laser energy was 250 mJ and the laser repetition rate was 3 Hz. The morphology and SAED pattern of the GNs are demonstrated in Fig. S1 (Supporting Information). 400 mg of $AgNO_3$ was dissolved in 30 mL of ethylene glycol with 10 mL of H_2O. This mixture was then added to the mixture of GNs/ethylene glycol and kept at 50 °C for 4 h. 40 ml of 0.1 mol/L sodium borohydride ($NaBH_4$) solution was slowly added and the mixture was heated at 110 °C for 2 h. Consequently, the reaction mixture was filtered and washed three times with distilled water, and finally dried in an oven at 80 °C under vacuum.

2.2 Fabrication of Pt, GNs and hybrid Ag/GNs CEs, and assembly of DSSCs

The FTO glasses were firstly cleaned in a detergent solution using an ultrasonic bath for 15 min and then respectively rinsed with ethanol and DI water. Then, both GNs solution and Ag/GNs solution were coated on FTO substrates, and dried at 70 °C. The state-of-the-art Pt CE was prepared by the thermal reduction method, in which a Pt precursor ($H_2PtCl_6{\cdot}H_2O$) was drop-casted on the FTO glass, followed by thermal treatment at 450 °C for 20 min.[7] The TiO_2 electrodes were fabricated by a screen-printing method and gradually sintered at 450 ℃ for 10 min after each printing. Then, the TiO_2 photoanodes were immersed in 0.5 mM N719 dye solution in a mixture of acetonitrile and tert-butyl alcohol (volume ratio: 1:1) at room temperature for 24 h to complete the sensitizer uptake, as described in our previous report.[7] The dye-sensitized TiO_2 photoanodes were subsequently washed with acetonitrile and further sandwiched with the fabricated CEs. The intervening space in the sandwich-type cell was filled with a drop of the electrolyte (0.60M BMII, 0.03M I_2, 0.10M guanidinium thiocyanate and 0.50M 4-tert-butylpyridine in the mixture of acetonitrile and valeronitrile (volume ratio: 85:15)).

2.3 Characterization

The morphology of the hybrid CEs was examined by scanning electron microscopy (SEM, JSM-7000F) and transmittance electron microscopy (TEM, JEOL-1400) The electrochemical responses (CV and EIS) were investigated by an electrochemical station (CH Instruments, CHI660B). Cyclic voltammetry (CV) measurements were carried out at a scan rate of 50 mV s^{-1} in a three-electrode system consisting of Pt wire as a CE, Ag/AgCl as a reference electrode and the various catalytic electrode materials coated FTO substrates as the working electrodes in the potential window of −0.2 to 0.8 V in acetonitrile solution containing 5 mM LiI, 0.5 mM I_2 and 0.1 M $LiClO_4$. The electrochemical impedance spectra (EIS) of various CEs were performed with a frequency range from 100 kHz to 0.1 Hz in a symmetric sandwich cell configuration. The photocurrent–voltage characteristics of DSSCs were performed under AM 1.5, 100 mW cm^{-2} illumination using a solar light simulator (Sun 2000). The incident photo-to-current conversion efficiencies (IPCE) were plotted as a function of wavelength from 300 to 800 nm using a QE/IPCE test system (Solar Cell Scan100, Zolix).

3. Results and discussion

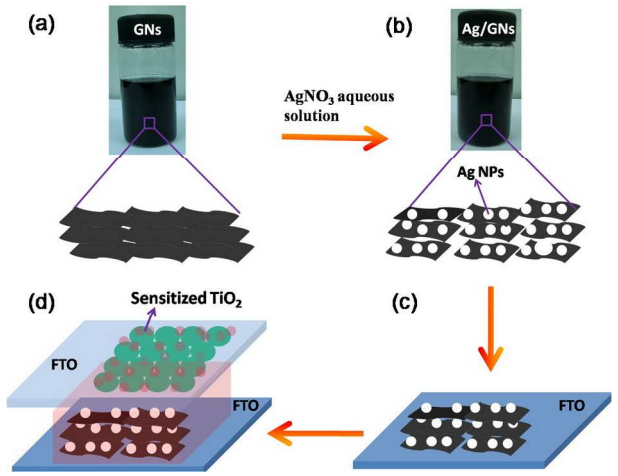

Fig.1 Overall procedure for the fabrication of hybrid Ag/GNs CEs for DSSCs. (a) well dispersed GNs precursor solutions. (b) Ag/GNs hybrids solution. (c) Ag/GNs solution loaded on the FTO substrate. (d) Application of hybrid Ag/GNs CEs in DSSCs.

The synthetic procedure of the electrodes and the assembly of a DSSC are illustrated in Fig. 1. GNs solution (Fig. 1a) was synthesized by pulsed laser reduction,[20] and the Ag/GNs composite solution (Fig. 2b) was prepared using a similar method reported by Z. Z. Yu *at el*.[21] Then, the prepared Ag/GNs hybrids were coated onto the FTO substrate as the CE materials for a DSSC, which was assembled with a dye N719 sensitized TiO_2 as the photoanode.[7]

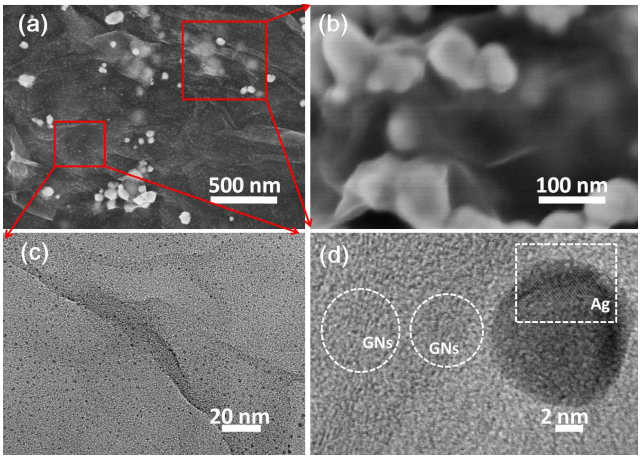

Fig.2 (a) SEM image of the Ag/graphene hybrids; (b) magnified SEM images of the big red square region in (a); (c) high-magnification TEM of the small red square region in (a), and (d) HR-TEM images of Ag/graphene composite.

The Ag/GNs hybrids with four kinds of different concentrations of Ag nanoparticles were fabricated. Fig. 2 shows scanning electron microscopy (SEM) and transmission electron microscopy (TEM) images of the optimized as-prepared Ag/graphene hybrids compared with Fig. S2 (Supporting Information). It can be seen from Fig. 2a and Fig. S1a (Supporting Information) that small Ag nanoparticles are closely anchored on the surface of graphene nanosheets though there are some agglomerations of Ag nanoparticles. Especially, many bright and dim white spots of aggregated Ag nanoparticles as shown in Fig. 2b exhibited the direct evidence that Ag nanoparticles have been supported on and inserted into both sides of the GNs. Namely, the Ag nanoparticles act as zero-dimensional nanospacers to lift the interspacing layer between individual GNs, forming a unique three-dimensional framework as shown in the magnified SEM images (Fig. 2b). Fig. 2c shows the high-magnification TEM of the small red square region in Fig. 2a. It clearly reveals that smaller Ag nanoparticles are firmly attached to the graphene nanosheets, even after the ultrasonication used to disperse the Ag/GNs composite for TEM characterization, suggesting the strong interaction between Ag nanoparticles and graphene nanosheets. The high-resolution TEM image in Fig. 2d shows the interfacial structure between GNs and the Ag nanoparticles, demonstrating the strong anchoring of Ag nanoparticles on graphene nanosheets, which enables fast electron transport through Ag nanoparticles to the underlying graphene layers to improve the electrochemical performance. Besides, due to the different size of Ag nanoparticles, the resultant effect on the electrocatalytic activity of Ag/GNs hybrids was reflected in Fig. S3 and Fig. S4 (Supporting Information). Compared with the fresh GNs consisting of randomly aggregated and crumpled sheets due to the π-π interaction between the large basal graphene planes, as shown in Fig. S1a (Supporting Information),[19] the Ag nanoparticles between the layers of graphene nanosheets can act as zero-dimensional nanospacers to efficiently prevent the closely restacking of graphene sheets, reducing the loss of their high active sites for I_3^-/I^- redox reaction.

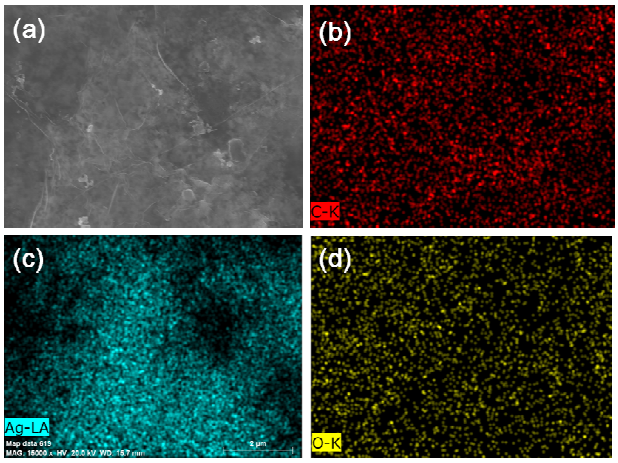

Fig.3 (a) SEM image of the selected area from the optimized Ag/GNs hybrids; (b-d)The EDX mapping of C (red), Ag (green), and O (yellow) elements in the same Ag/GNs region.

To further verify the distribution of the elements in the optimized Ag/GNs hybrids, EDX element mapping was used to understand the distribution of Ag nanoparticles in the hybrids as shown in Fig. 3. Fig. 3(a) shows the original SEM image of the selected area from the optimized Ag/GNs used for the EDX mapping. Fig. 3(d–f) display the corresponding C, Ag and O element mapping, which indicate a relatively homogeneous distribution over the entire Ag/GNs except for some cavities without GNs. Besides, most Ag nanoparticles are prone to successfully inserting and lifting the layers of GNs, and thus the graphene layers are hybridized with these nanoparticles to preserve a three-dimensional laminated structure of the GNs [19], which is believed to offer additional active sites and cavities available for I_3^-/I^- insertion.

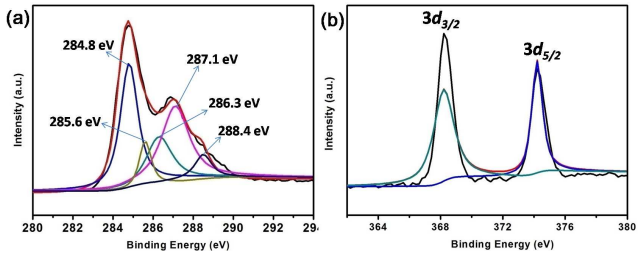

Fig.4 (a) C1s and (b) Ag3d XPS spectra of the optimized Ag/GNs hybrids.

Fig. 4 shows the C1s and Ag3d XPS spectra of the optimized Ag/GNs hybrids. The C1s spectrum (Fig. 4a) exhibits five fitting curves centered at 284.8 eV (C=C/C–C in aromatic ring), 285.6 eV (C–OH), 286.3 eV (C–O–C), 287.1 eV (C=O) and 288.4 eV (HO–C=O) [21]. The C1s XPS spectrum of the GNs clearly indicated the considerable reduction of GO.[18] The peak corresponding to sp^2 C–C (~284.8 eV) is majorly observed, which implies significant recovery of the basal plane of the GNs after the pulsed laser reduction. Fig. 4b demonstrates the Ag XPS spectrum of the as-prepared Ag/GNs hybrids. The binding energies in the XPS spectra presented in Fig. 4b are calibrated by C1s (284.8 eV). The peaks appearing in Fig. 4b are attributed to $Ag^{3d5/2}$ (367.2 eV) and $Ag^{3d3/2}$ (373.2 eV), respectively. It is worthwhile to mention that the peak positions of Ag^{3d} shift remarkably to the lower binding energy compared with that of bulk Ag ($Ag^{3d5/2}$, 368.3 eV; and $Ag^{3d3/2}$, 374.3 eV32), which is ascribed to the electron transfer from metallic Ag to GNs,[22] indicating that there is a strong interaction between Ag nanoparticles and GNs. Therefore, in combination with the EDX mapping (Fig. 3c), it can be concluded that the as-synthesized Ag/GNs hybrids possess the well dispersity of Ag nanoparticles.

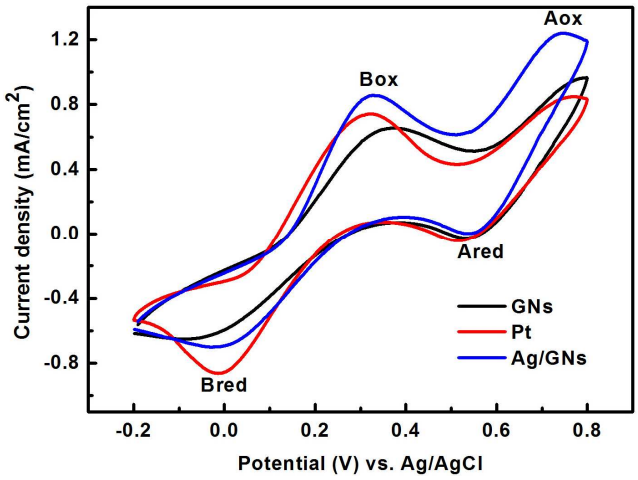

Fig.5 Cyclic voltammograms of GNs, optimized Ag/GNs hybrids and thermally platinized FTO CEs at a scan rate of 50 mV/s in an acetonitrile solution containing 5 mM LiI, 0.5 mM I_2 and 0.1 M $LiClO_4$. The counter electrode was a Pt wire and the reference electrode was Ag/AgCl.

Cyclic voltammetry (CV) is a powerful tool to investigate the electrocatalytic activity of CEs. The three types of synthesized CEs were placed in an acetonitrile solution containing 5 mM LiI, 0.5 mM I_2 and 0.1 M $LiClO_4$. The deposition area for all the CEs is ~ 0.64 cm^2. As shown in Figure 4a, two pairs of oxidation/reduction peaks, A_{ox}/A_{red} and B_{ox}/B_{red}, correspond to the reactions in Equation (1) and (2), respectively,[23,24] are observed in the CV curves for each CE.

$$3I_2 + 2e^- \rightarrow 2I_3^- \quad (1)$$

$$I_3^- + 2e^- \rightarrow 3I^- \quad (2)$$

The left pair of peaks, which show the I^-/I_3^- redox process, is of interest for the performance of CEs. The peak-to-peak separation (E_{pp}) of the left pairs can elucidate redox reaction kinetics at the CEs. Compared with the E_{pp} (331 mV) of Pt CE, the GNs CE shows a much wider E_{pp} (450 mV), indicating GNs CE owns a slower redox reaction rate. However, the value of E_{pp} (349 mV) is reduced considerably in the Ag/GNs CE and is nearly comparable to that of the Pt CE. This fact implies that incorporating Ag nanoparticles into GNs can significantly reduce the overpotential for the I_3^- reduction, resulting in the enhancement of the reaction kinetics.[25,26] In addition, the current density, which is closely related to the amount of redox reaction occurring on the CEs, was significantly increased in the Ag/GNs hybrid CE.[12,27] Furthermore, the long term stability of prepared Ag/GNs CE was conducted after continuous CV, as shown in Fig. S5 (Supporting information). Considering that the Ag nanoparticles act as zero-dimensional nanospacers to lift the interspacing layer between individual GNs, therefore, this enhanced redox reaction is mainly ascribed to a unique three-dimensional framework of the Ag/GNs CE (Fig. 2a), which efficiently prevents the multilayered agglomerate and restacking of graphene layers. Compared to the aggregated GNs, this desirable three-dimensional framework significantly increases the amount of active sites accessibility for the redox reaction of I^-/I_3^- on the Ag/GNs hybrid CE.[11,15,19].

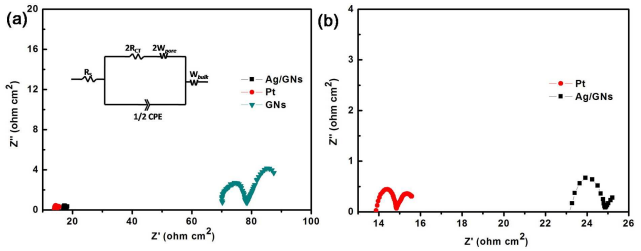

Fig.6 (a) Electrochemical impedance spectra (EIS) of GNs, optimized Ag/GNs hybrids and Pt CEs in a symmetric sandwich cell configuration, and the inserted figure shows the equivalent circuit diagram for fitting the EIS (R_S is the series resistance, R_{CT} is the charge transfer resistance at the CE/electrolyte interface, W_{pore} is the Warburg impedance within CE layers, CPE is constant phase element of one electrode, and W_{bulk} is the Warburg impedance between the two CEs.); (b) The magnified EIS of Pt CE and Ag/GNs CE from (a).

The electrocatalytic performance of the prepared films on the reduction of I_3^- ions was characterized using electrochemical impendence spectroscopy (EIS). The Nyquist plots of various symmetrical cells are shown in Fig. 6a. For the symmetric cells, the identical GNs and Ag/GNs CEs were used as the working electrodes, in which the electrolyte solution containing I^-/I_3^- redox couples was filled in between. The magnified EIS spectra of symmetric cells with Ag/GNs and Pt CEs are displayed in the Fig. 6b. Generally, the high frequency semicircle indicates the electrochemical charge transfer resistance (R_{CT}) at the CE/electrolyte interface, whereas the low-frequency semicircle indicates Nernst diffusion-limited impedance of the I^-/I_3^- redox species in the electrolyte (R_D).[1,2] The plots were fitted with an equivalent circuit, as shown in the inset of Fig. 6a, consisting of the R_{CT} in parallel with a constant phase element (CPE), both of which are in series with the Warburg impedance within electrode pores (W_{pore}) and sheet resistance (R_S). Especially, the R_{CT}

represents the catalytic property of the CE. As mentioned before in CV, the introduction of the Ag nanoparticles into the GNs electrode leads to an obvious improvement in the electrocatalytic activity due to providing a more active sites. We found that the R_{CT} value on the GNs CE/electrolyte interface of the symmetric cell was ~ 10 Ω cm^2. Whereas, after the Ag nanoparticles were introduced into the GNs, the R_{CT} value (~ 1.02 Ω cm^2) obtained from the optimized Ag/GNs hybrid CE is ~10 times lower than that of the GNs CEs. This result obviously proved that Ag/GNs hybrids have more active sites for the reduction of I_3^- than that of pure GNs.

Table 1. Photovoltaic parameters of DSSCs fabricated with GNs, optimized Ag/GNs hybrids and Pt CEs

CE	R_{CT}/Ω cm^2	J_{SC}/mA cm^{-2}	V_{OC}/V	FF/%	η/%
GNs	10.0	14.22	0.665	51	4.87
Ag/GNs	1.02	14.67	0.732	72	7.72
Pt	0.76	16.24	0.733	69	8.25

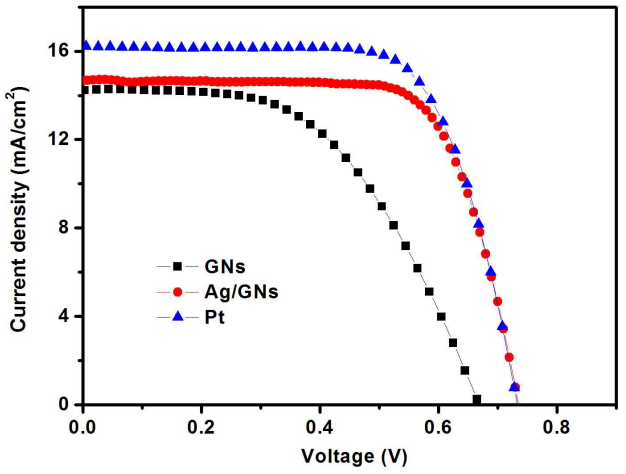

Fig.7 Photocurrent–voltage characteristics of DSSCs with GNs, optimized Ag/GNs hybrids and Pt CEs measured under AM 1.5 simulated solar illuminations.

DSSCs were fabricated to demonstrate the performance of various CEs in a practical application. Fig. 7 shows the current density-voltage (J–V) characteristics of the DSSCs using various CEs under one sun illumination (AM 1.5G, 100 mW cm^{-2}). The device photovoltaic parameters are summarized in **Table 1**. The values of Jsc, FF and Voc of the DSSC using Ag/GNs as the CE increase compared with those using GNs as the CE. Generally, R_{CT} can significantly affect the device performance in two ways: (1) lower R_{CT} leads to lower total internal resistance, which is better for the FF; (2) lower R_{CT} also implies effective reduction of I_3^- to I^- at the electrolyte–CE interface, which could favor the dye-regeneration process at the electrolyte–photoanode interface, reflected in the improvement of J_{SC}.[6]As shown in Fig. 6, the R_{CT} of the Ag/GNs CE was ten times less than that of the GNs CE, therefore the improved Jsc and relatively high FF of Ag/GNs were attributed to the low R_{CT} due to its three-dimensional hybrids nature according to the results of SEM (Fig. 2a and 2b) and CV (Fig. 5). Compared with GNs CE, the low diffusion impedance of Ag/GNs hybrids CE results in the relatively high V_{OC}.[3] Besides, Figure S6 (Supporting Information) shows the incident photon to charge carrier efficiency (IPCE) for DSSCs with GNs, Ag/GNs, and Pt CEs, respectively. As expected, the Ag/GNs with three-dimensional hybrid framework show relatively high IPCE compared to the aggregated GNs. Furthermore, table S1 (Supporting Information) exhibits the long term stability of DSSC cells with a CE of Ag/GNs. The power conversion efficiency (η= 7.72%) of the cells using the Ag/GNs hybrids with high IPCE as a CE, which is comparable to that (η= 8.25%) of DSSCs using state-of-the-art Pt-CEs, was approximately two times higher than that (η= 4.87%) of the cells using GNs CE. Additionally, compared with the best η (6.81%) reported by Huang *et al* using GNs CEs,[10] the enhancement of η is due to its three-dimensional hybrid framework with enhanced electrochemical catalytic activity and high conductivity by the Ag nanoparticles as zero-dimensional nanospacers inserting into GNs. According to the high efficiency DSSCs with 3D N-doped graphene foams (N-GFs) and 3D honeycomb-like structured graphene sheets as CEs synthesized by Dai[28] and Hu[29] et al, this unique 3D hybrid structure design efficiently prevents the agglomerations and restacking of GNs, and further increase the active sites for the I_3^-/I^- electrocatalysis.

4. Conclusion

Highly efficient hybrid CEs incorporating Ag nanoparticles and GNs were fabricated. The Ag nanoparticles, serving as zero-dimensional nanospacers inserting into the graphene framework, were well dispersed on the surfaces of the GNs. This novel hybrid system has been proved that the GNs were efficiently isolated from each other by Ag nanoparticles to prevent the aggregation and restacking of GNs, which increase the active defective sites for the redox reaction of I^-/I_3^-. The superior electrocatalytic response of the Ag/GNs hybrids CE can be ascribed to a low charge transfer resistance and an extended interlayer distance due to the insertion of zero-dimensional Ag nanoparticles into GNs. The DSSCs with the optimized Ag/GNs hybrid CE shows high energy conversion efficiency (7.72%), which is comparable to that of devices using the state-of-the-art Pt CEs (8.25%).

Acknowledgements

This work has been partly supported by the National Natural Science Foundation of China (No.50972091), 863 project grants (2013AA031502), the National Science Foundation (No. 51202046), the Fundamental Research Funds for the Central Universities (No. HIT. NSRIF. 2013006), and Program for New Century Excellent Talents in University (NCET-10-0066), the Shanghai Municipal Science & Technology Commission key supporting project (No.12120502900) and industrial research fund from Wuhu Token Sciences Co., Ltd. Prof. Lei Huang appreciates the support of The Program for Professor of Special Appointment (Eastern Scholar) at Shanghai Institutions of Higher Learning.

Notes and references

[a] *Department of Opto-electric Information Materials and Quantum Devices, School of Materials Science and Engineering, Harbin Institute of Technology, 150001 Harbin, China.*
E-mail: jinzhong_wang@hit.edu.cn (J. Wang).
Tel.: +86 451 86418745; fax: +86 451 86418745.
[b] *Joint Lab with Wuhu Token for Graphene Electrical Materials and Application, Department of Physics, Shanghai Normal University, Guilin Road 100, Shanghai 200234, China.*
E-mail: leihuang@shnu.edu.cn; elhuang68@yahoo.com.sg;
Tel.: +86 21 6432 8968; Fax: +86 21 6432 8968.
These authors contributed equally to this work.
† Electronic Supplementary Information (ESI) available: [details of any supplementary information available should be included here]. See DOI: 10.1039/b000000x/

[1]V. D. Dao, L. L. Larina, K. D. Jung, J. K. Lee, H. S. Choi, Nanoscale, , 2014, **6**, 477.
[2]V. D. Dao, N. T. Q. Hoa, L. L. Larina, J. K. Leed, H. S. Choi, Nanoscale, 2013, **5**, 12237.
[3] G. R. Li, J. Song, G. L. Pan, X. P. Gao, Energy Environ. Sci., 2011, **4**, 1680.
[4] X.K. Xin, M. He, W. Han, J. Jung, Z.Q. Lin, Angew. Chem. Int. Ed. 2011, **50**, 11739.
[5] Q.D. Tai, B.L. Chen, F. Guo, S. Xu, H. Hu, B. Sebo, X.Z. Zhao, ACS Nano, 2011, **5**, 3795.
[6]S.C. Hou, X. Cai, H.W. Wu, X. Yu, M. Peng, K. Yan, D.C. Zou, Energy Environ. Sci., 2013, **6**, 3356.
[7] Y. Yan, J. Z. Wang, Q. H. Chang, M. Babikier, H. X. Wang, H. T. Li, Q. J. Yu, S. Y. Gao, S. J. Jiao, Electrochim. Acta, 2013, **94**, 277.
[8]T. Krishnamoorthy, M. Z. Tang, A. Verma, A. S. Nair, D. Pliszka, S. G. Mhaisalkard, S. Ramakrishna, J. Mater. Chem., 2012, **22**, 2166.
[9] C. T. Yip, M. Guo, H. T. Huang, L. M. Zhou, Y. Wang, C. J. Huang, Nanoscale, 2012, **4**, 448.
[10] D. W. Zhang, X. D. Li, H. B. Li, S. Chen, Z. Sun, X. J. Yin, S. M. Huang, Carbon, 2011,**49**, 5382.
[11] L. Kavan, J. H. Yum, M. K. Nazeeruddin, M. Grätzel, ACS Nano, 2011, **5**, 9171.
[12] J. D. Roy-Mayhew, D. J. Bozym, C. Punckt, I. A. Aksay, ACS Nano, 2010, **4**, 6203.
[13]H. Choi, H. Kim, S. Hwang, Y. Han, M. Jeon, J. Mater. Chem., 2011, **21**, 7548.
[14] L. Kavan, J. H. Yum, M. Grätzel, ACS Nano, 2011, **5**, 165.
[15] G. Veerappan, K. Bojan, S. W. Rhee, Appl. Mater. Interfaces, 2011, **3**, 857.
[17] X. S. Du, Z. Z. Yu, A. Dasari, J. Ma, M. Mo, Y. Z. Meng, Y. W. Mai, Chem. Mater., 2008, **20**, 2066.
[18] L. H. Chang, C. K. Hsieh, M. C. Hsiao, J. C. Chiang, P. I. Liu, K. K. Ho, C. C. M. M, M. Y. Yen, M. C. Tsai, C. H. Tsai, Journal of Power Sources, 2013, **222**, 518.
[19] C. T. Hsieh, C. Y. Lin, Y. F. Chen, J. S. Lin, H. Teng, Carbon, 2013, **6**, 109.
[20] L. Huang, Y. Liu, L. C. Ji, Y. Q. Xie, T. Wang, W. Z. Shi, Carbon, 2011, **49**, 2431.
[21] X. Z. Tang, X. F. Li, Z. W. Cao, J. L. Yang, H. Wang, X. Pu, Z. Z. Yu, Carbon, 2013, **59**, 93.
[22] X. F. You, F. Chen, J. L. Zhang, M. Anpo, Catalysis Letters, 2005, **102**, 3.
[23]Z. S. Wu, G. M. Zhou, L. C.Yin, W. C. Ren, F. Li, H. M. Cheng, Nano Energy, 2012, **1**, 107.
[24] Z. Y. Zhang, X. Y. Zhang, H. X. Xu, Z. H. Liu, S. P. Pang, X. H. Zhou, S. M. Dong, X. Chen, G. L. Cui, Appl. Mater. Interfaces, 2012, **4**, 6242.
[25] Z. B. Yang, M. K. Liu, C. Zhang, W. W. Tjiu, T. X. Liu, H. S. Peng, Angew. Chem. Int. Ed., 2013, **52**, 3996.
[26] Z. B. Yang, L. Li, Y. F. Luo, R. X. He, L. B. Qiu, H. J. Lin, H. S. Peng, J. Mater. Chem., A, 2013, **1**, 954.
[27] Y. Q. Sun, Q. Wu, G. Q. Shi, Energy Environ. Sci., 2011, **4**, 1113.
[28]Y.H. Xue, J. Liu, H. Chen, R.G. Wang, D.Q. Li, J. Qu, L.M. Dai, Angew. Chem. Int. Ed. 2012, **51**, 12124 .
[29] H. Wang, K. Sun, F. Tao, D.J. Stacchiola, Y.H. Hu, Angew. Chem. Int. Ed. 2013, **52**, 9210.